# Mars Entry, Descent and Landing Parametric Trades

Grant Wells*
*Georgia Institute of Technology, Atlanta, GA 30332*

**The purpose of this investigation is to begin forming a dataset to be the basis of a Mars entry, descent and landing mission design handbook for planetary probes. The premise of the project is that Mars entry, descent and landing can be parameterized with five variables: (1) entry mass, (2) entry velocity, (3) entry flight path angle, (4) vehicle aeroshell diameter, and (5) vertical lift-to-drag ratio. For combinations of these input parameters, the following trajectory information will be determined: peak deceleration, peak heat rate, heat load, and the altitude at which Mach 2 is reached (for parachute deployment).**

## I. Introduction

THE purpose of this investigation is to begin forming a dataset to be the basis of a Mars entry, descent and landing (EDL) mission design handbook for planetary probes. The Mars EDL mission design handbook would serve as the initial basis for planetary probe EDL in the same manner that a Mars interplanetary mission design handbook serves as the initial basis for launch vehicle selection and mission timelines. As with interplanetary mission design handbooks, an EDL mission design handbook could be constructed for each planet of interest.

The premise of this investigation is that Mars EDL can be parameterized with five variables: (1) entry mass, (2) entry velocity, (3) entry flight path angle, (4) vehicle aeroshell diameter, and (5) vertical lift-to-drag ratio. For combinations of these input parameters, the following trajectory information would be determined: peak deceleration, peak heat rate, total heat load, and the altitude at which Mach 2 is reached (for parachute deployment). The data would then be assembled and presented as a series of "pork chop" (contour) plots with the five EDL variables on the x and y axes and the trajectory information shown by the contours.

The central idea is that if a mission designer knows the entry conditions, size and aerodynamic properties for a particular planetary probe, the peak deceleration, peak heat rate, total heat load, and the altitude at which Mach 2 is reached for the trajectory can all be determined without having to run trajectory simulations. Similarly, the effects on the trajectory due to changes in the input parameters could quickly be determined. For example, the change in the Mach 2 altitude from an increase in entry mass could quickly be assessed.

## II. Methodology

### A. Major Variables

Ranges for the five parameters used to characterize Mars entry are shown in Table 1. The maximum value of the entry mass range was chosen based the expected entry mass for the Mars Science Lander (MSL) of approximately 2000 kg[1], which is currently the heaviest Martian planetary probe planned. The range of entry velocities and flight path angles were chosen to encompass the range of entry velocities seen by several successful probes, specifically for entry velocity: Viking 1 (4.61 km/s)[2] and Pathfinder (7.26 km/s)[3] and for entry flight path angle: Viking 2 (-17.027°)[2] and the Mars Exploration Rovers (MERs) (-11.5°)[4]. The range of aeroshell diameters bounds probes from Pathfinder (2.65 m)[3] to the largest probe which can pass through the environmental test chamber at the Jet Propulsion Laboratory (approximately 4.5 m allowing for handling equipment). The range of vertical lift-to-drag ratios encompasses ballistic entry (0) to a possible maximum value for blunt bodies (0.5).

The reference areas corresponding to the individual diameters are shown in Table 2. Since both entry mass and aeroshell diameter are independent parameters in this investigation, a wide ballistic coefficient range is assessed as shown in Table 3. An alternative approach to this investigation might have been to use either entry mass or diameter as one independent variable and a packing density as the other variable. Packing density is a measure of how much mass could be put into an aeroshell of a given shape. The packing density could be used to determine either the

* Graduate Research Assistant, Daniel Guggenheim School of Aerospace Engineering, Georgia Institute of Technology, 270 Ferst Drive, Atlanta, GA 30332-0150.

aeroshell diameter for a given entry mass (by photographically scaling the aeroshell), or the entry mass for a given diameter of the aeroshell (by increasing the mass until the desired packing density was reached). The shaded ballistic coefficients in Table 3 show the range of values for a low packing density based on Viking and a high packing density based on MER.

**Table 1 Ranges for the variables used to characterize Mars entry.**

| Input Parameter | Minimum | Maximum | Increment |
|---|---|---|---|
| Entry Mass (kg) | 200 | 2000 | 200 |
| Entry Velocity (km/s) | 4 | 9 | 1 |
| Entry Flight Path Angle (°) | -25 | -10 | 5 |
| Aeroshell Diameter (m) | 2 | 5 | 1 |
| Lift-to-Drag Ratio | 0 | 0.5 | 0.1 |

**Table 2 Aeroshell diameters and corresponding reference areas.**

| Diameter (m) | Reference Area ($m^2$) |
|---|---|
| 1 | 0.79 |
| 2 | 3.14 |
| 3 | 7.07 |
| 4 | 12.57 |
| 5 | 19.63 |

**Table 3 Ballistic coefficients based on entry mass and aeroshell diameter.**

| Ballistic Coefficient ($kg/m^2$) | | Diameter (m) | | | |
|---|---|---|---|---|---|
| | | 2 | 3 | 4 | 5 |
| Mass (kg) | 200 | 37.9 | 16.8 | 9.5 | 6.1 |
| | 400 | 75.8 | 33.7 | 18.9 | 12.1 |
| | 600 | 113.7 | 50.5 | 28.4 | 18.2 |
| | 800 | 151.6 | 67.4 | 37.9 | 24.3 |
| | 1000 | 189.5 | 84.2 | 47.4 | 30.3 |
| | 1200 | 227.4 | 101.1 | 56.8 | 36.4 |
| | 1400 | 265.3 | 117.9 | 66.3 | 42.4 |
| | 1600 | 303.2 | 134.7 | 75.8 | 48.5 |
| | 1800 | 341.0 | 151.6 | 85.3 | 54.6 |
| | 2000 | 378.9 | 168.4 | 94.7 | 60.6 |

### B. Commonalities between Trajectory Simulations

All 5760 trajectories were simulated using the Program to Optimize Simulated Trajectories (POST[5]). Each planetary probe was assumed to have a constant hypersonic drag coefficient of 1.68[6] typical of 70°-sphere-cone planetary probes. The vertical lift coefficient for the vehicle was determined by multiplying the drag coefficient with the vertical lift-to-drag ratio. For vehicles in banked flight, the lift coefficient would represent the portion of lift in the vertical direction.

All trajectory simulations used a common atmosphere. The atmospheric density on Mars varies significantly with time-of-year, time-of-day, dust-level (atmospheric opacity) and latitude. To account for the effects of each of these variables, a design atmospheric density profile was constructed from approximately one-thousand runs of Mars-GRAM 2005[7] in which month, time of day, dust level, and latitude for the years of 2030 and 2031 were randomly varied. The results of the Mars-GRAM runs covered the range of densities shown in Figure 1.

A cumulative distribution function of density was constructed for 0 km MOLA. The density at the 30% point on the 0 km cumulative distribution function (0.0124 kg/m³) as shown in Figure 1 was chosen as the basis for the atmosphere. The atmosphere from the Mars-GRAM 2005 runs having a 0 km density of 0.0124 kg/m³ with the lowest 4 km density was then chosen for this investigation. The resulting atmosphere (shown in Figure 2) was chosen for this investigation.

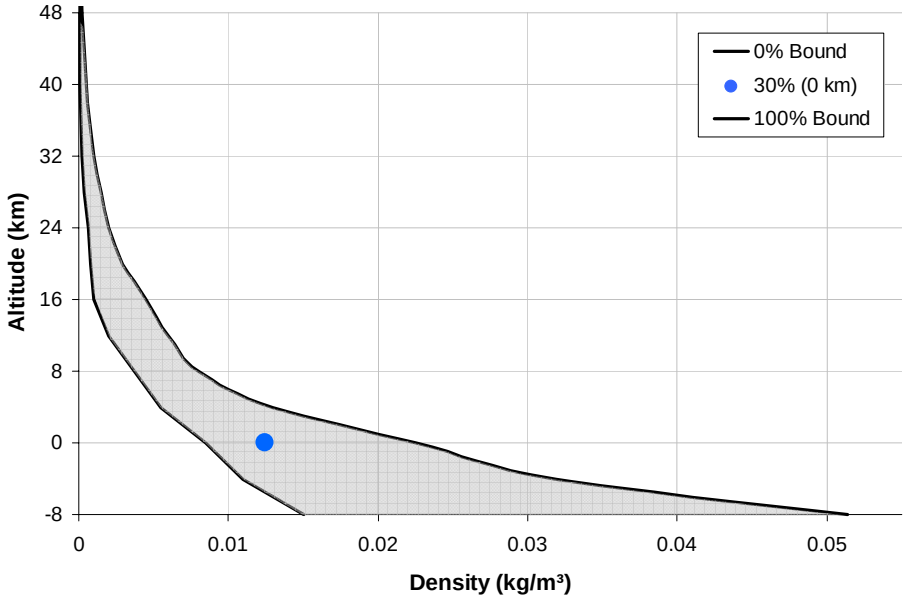


**Figure 1 The range of densities resulting from over 1000 runs of Mars-GRAM 2005.**

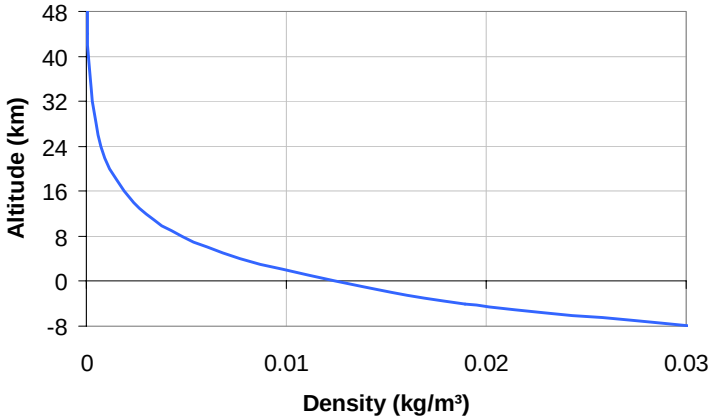


**Figure 2 Martian atmospheric density profile used for trajectory simulations.**

### C. Plots of Trajectory Data

After a trajectory for one combination of the input variables shown in Table 1 was run, the peak deceleration, peak heat rate, heat load, and Mach 2 altitude (for parachute deployment) were recorded. This data was then plotted against two of the major input variables (e.g. entry mass and flight path angle), while the other three major input variables (e.g. entry velocity, aeroshell diameter, and lift-to-drag ratio) were held constant. The data takes the form of contours in the plot such as that shown in Figure 3 for peak deceleration.

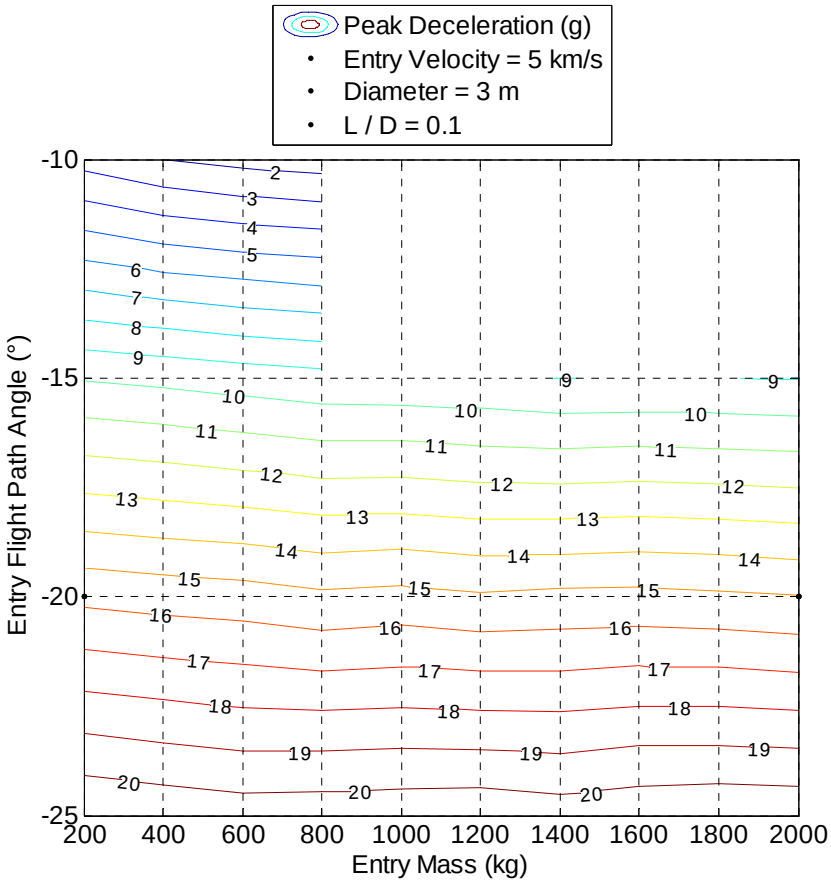


**Figure 3 An example plot of peak deceleration. The blank region between 800 and 2000 kg and -10° and -15° represents a region where the trajectory showed the probe skipping out of the atmosphere for a flight path angle of -10°, so contours cannot be plotted in this region.**

Intersections of the gridlines on the contour plots show the specific points for which a trajectory simulation was run. Blank regions of the contour plots indicate combinations of major variables for which the simulations showed the probe skipping out of the atmosphere. Data was not recorded for cases which skipped out of the atmosphere. In order for contours to be plotted in any rectangular region bounded by the gridlines, the cases at the four vertices cannot have skipped out of the atmosphere, so contours cannot be plotted in these regions as shown in Figure 4.

For example, in Figure 3, the contour plot shows how peak deceleration varies with entry mass and flight path angle when entry velocity is held constant at 5 km/s, aeroshell diameter is held constant at 3 m, and the lift-to-drag ratio is held constant at 0.1. For this particular combination of entry velocity, aeroshell diameter, and flight path angle, the -10° flight path angle cases with masses from 1000 kg to 2000 kg skipped out of the atmosphere.

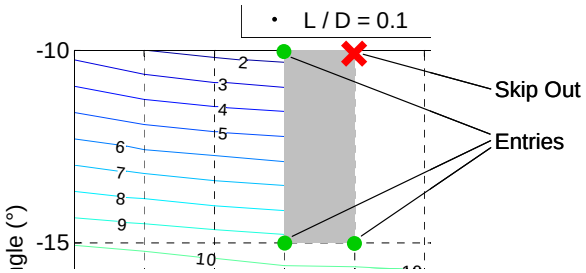


**Figure 4 Contour plots require successful entries for each of the four cases bounding regions of the plot.**

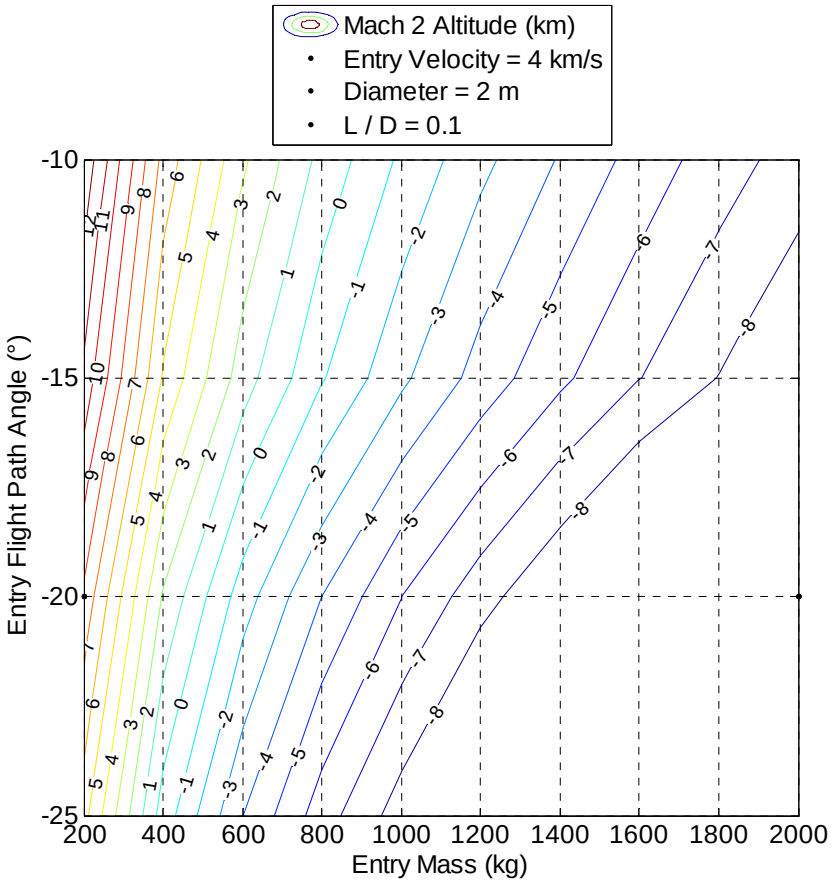


**Figure 5 An example plot of Mach 2 altitude. Mach 2 altitudes below -8 km were not plotted as the lowest point on Mars, located in Hellas Planitia, has an altitude of -8.18 km.[9]**

The lowest point on Mars[9] has an elevation of -8.18 km, so Mach 2 altitudes lower than -8 km were not plotted on the contour plots.

## III. Results

The following paragraphs discuss some trends that can be seen in the results of the trajectory simulations. A sampling of the contour plots for peak deceleration, peak heat rate, heat load, and Mach 2 altitude are shown below. Contour plots of the entire dataset can be found in the appendix. Note that plots were generally not made for combinations of variables which did not result in any successful entries that could be presented as a contour plot.

### A. Peak Deceleration

As can be seen from Figure 6, peak deceleration is generally not a strong function of entry mass when the entry velocity, aeroshell diameter, and lift-to-drag ratio are all fixed. Entry flight path angle, however, does significantly affect the peak deceleration of the entry trajectory when the other three major variables are fixed. Figure 7 shows that peak deceleration is also a strong function of entry velocity in addition to entry flight path angle for a fixed entry mass, aeroshell diameter, and lift-to-drag ratio.

When plotted against aeroshell diameter and entry mass as shown in Figure 8, peak deceleration shows some expected trends. For a fixed aeroshell diameter, peak deceleration decreases as entry mass increases since the drag force is fixed (i.e. the same amount of force causes less deceleration as mass increases). While for a fixed entry mass, increasing the aeroshell diameter increases the drag force and also the deceleration of the planetary probe.

For a fixed entry mass, entry velocity and lift-to-drag ratio, however, as shown in Figure 9, diameter does not significantly affect the peak deceleration.

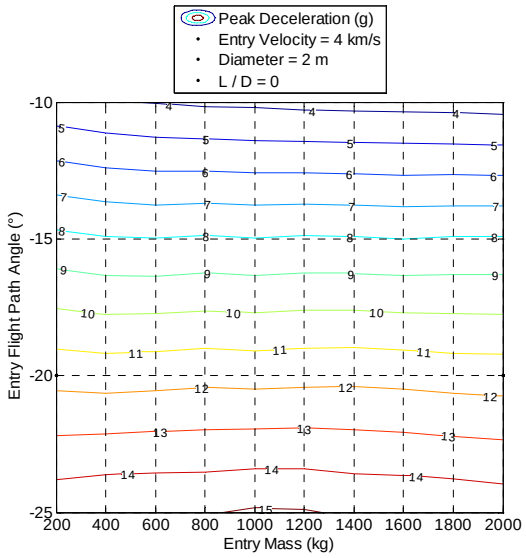


**Figure 6 Peak deceleration as a function of entry mass and flight path angle.**

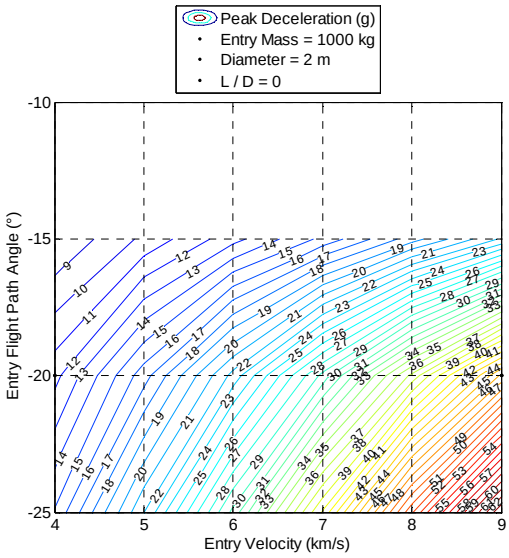


**Figure 7 Peak deceleration as a function of entry velocity and flight path angle.**

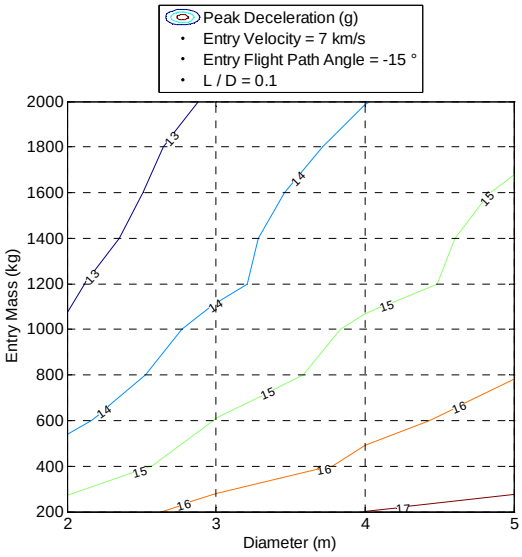


**Figure 8 Peak deceleration as a function of entry mass and aeroshell diameter.**

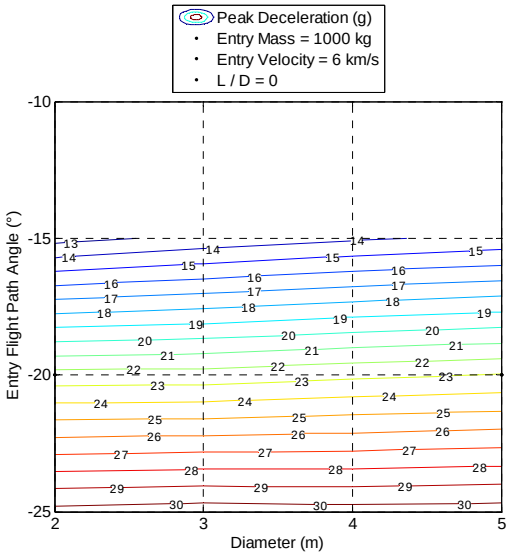


**Figure 9 Peak deceleration as a function of aeroshell diameter and entry flight path angle.**

Figure 10 shows that there is some decrease in peak deceleration as lift-to-drag ratio increases for a fixed entry mass, entry velocity, and aeroshell diameter. Figure 11 shows the significant effect that entry velocity has on peak deceleration for a fixed entry mass, entry flight path angle, and aeroshell diameter.

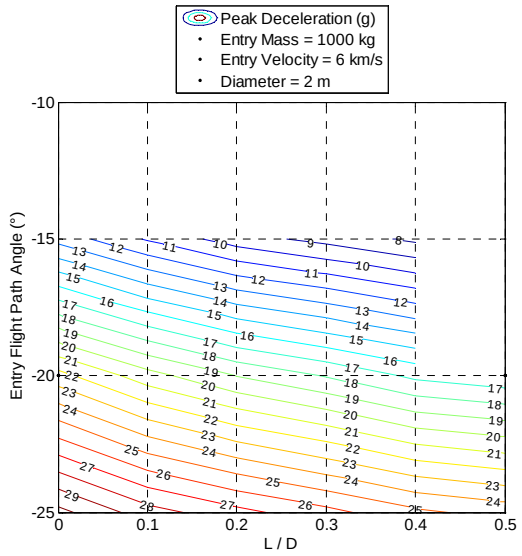


**Figure 10 Peak deceleration as a function of lift-to-drag ratio and entry flight path angle.**

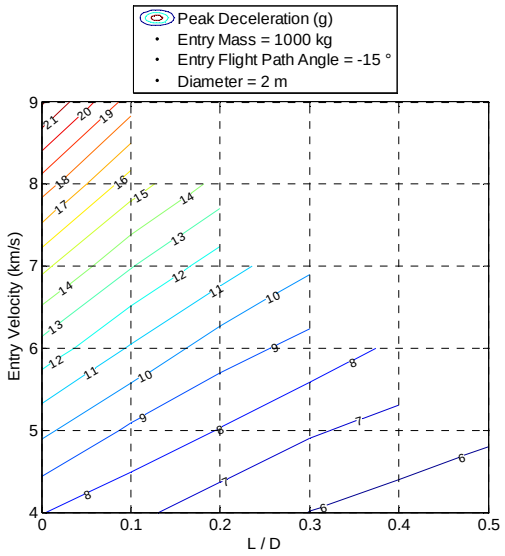


**Figure 11 Peak deceleration as a function of lift-to-drag ratio and entry velocity.**

## B. Peak Heat Rate

The laminar stagnation point heat rate was calculated for each trajectory. Radiative effects were included for entry velocities above 6 km/s.[8] Peak heat rate increases with entry mass and slightly increases with entry flight path angle as shown in Figure 12 for a fixed entry velocity, aeroshell diameter, and lift-to-drag ratio. Increasing entry velocity significantly increases peak heat rate as depicted in Figure 13 for a fixed entry mass, aeroshell diameter, and lift-to-drag ratio. This is as expected since the major variables affecting heat rate are velocity, atmospheric density and the stagnation point radius.

Peak heat rate significantly decreases as aeroshell diameter increases as shown in Figure 14. This is an expected result for this investigation, because the stagnation point radius used for heating calculations is equal to one-fourth of the aeroshell diameter for each case ($r_n = 0.25D$).

Figure 15 shows that for a fixed entry mass, aeroshell diameter, and entry velocity, decreasing the entry flight path angle more significantly reduces the peak heat rate than increasing the lift-to-drag ratio of the planetary probe.

Figure 16 shows that for a fixed entry mass, entry flight path angle, and aeroshell diameter, peak heat rate is nearly independent of lift-to-drag ratio, but a reduced entry velocity results in a reduced peak heat rate as expected.

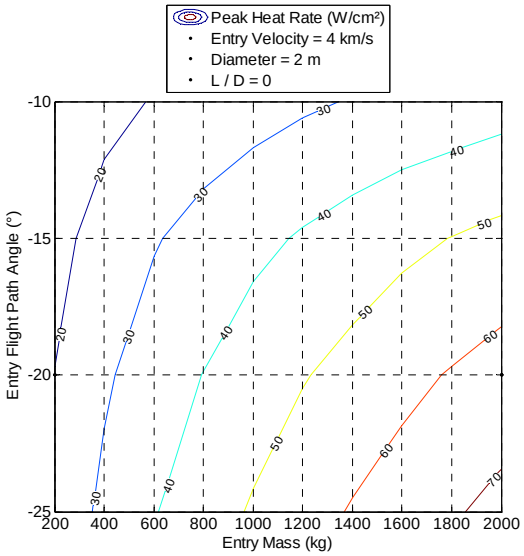


**Figure 12 Peak heat rate as a function of entry mass and flight path angle.**

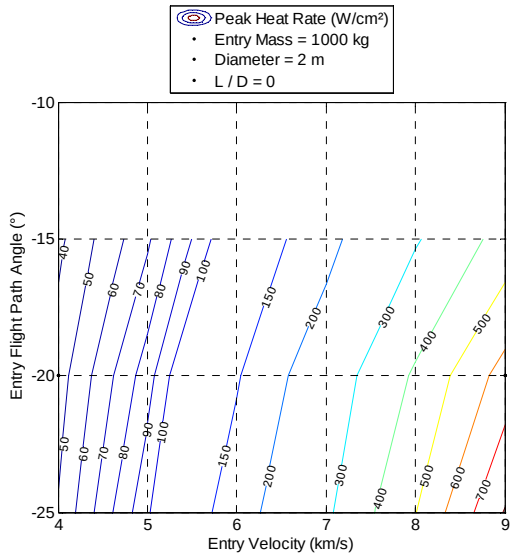


**Figure 13 Peak heat rate as a function of entry velocity and flight path angle.**

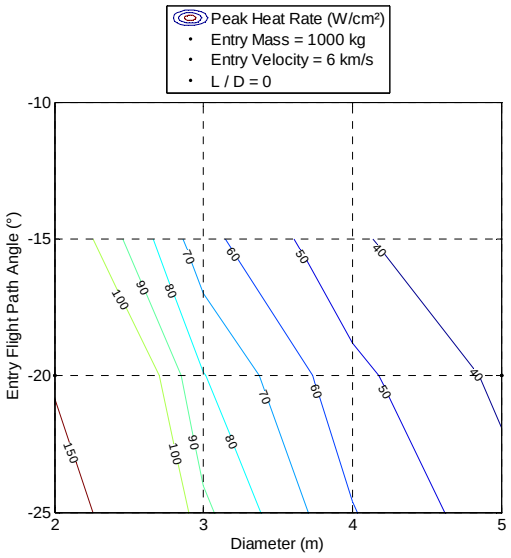


**Figure 14 Peak heat rate as a function of aeroshell diameter and entry flight path angle.**

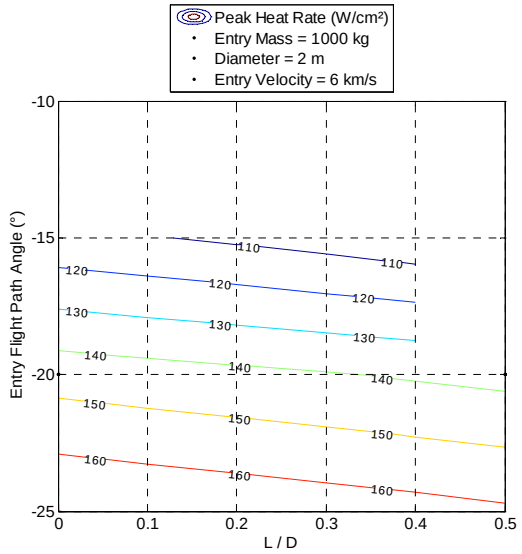


**Figure 15 Peak heat rate as a function of lift-to-drag ratio and entry flight path angle.**

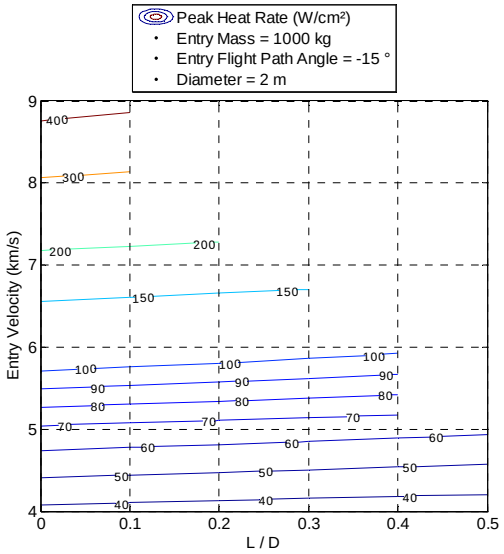


**Figure 16 Peak heat rate as a function of lift-to-drag ratio and entry velocity.**

## C. Heat Load

Figure 17 shows that heat load increases with entry mass and decreases with steepening of the entry flight path angle. As entry mass increases, heat load increases more quickly with entry mass at shallower entry flight path angles than at steeper flight path angles. Figure 18 also shows that heat load increases with both entry velocity and shallower flight path angles, though more so with entry velocity, due to the higher heat rates experienced by the planetary probe, for a fixed entry mass, aeroshell diameter, and lift-to-drag ratio.

Figure 19 shows that for a fixed entry flight path angle, entry mass, entry velocity, and lift-to-drag ratio, increasing the aeroshell diameter decreases the heat load of the planetary probe as expected due to the lower heating levels experienced by planetary probes with larger stagnation point radii. The effect of the steeper entry flight path

angle on reducing heat load is also evident.

As lift-to-drag ratio increases, Figure 20 shows that heat load increases slightly for a constant entry mass, entry velocity, and aeroshell diameter.

Figure 21 shows that heat load is not a strong function of lift-to-drag ratio for a fixed entry mass, entry flight path angle, and aeroshell diameter, though heat load does increase slightly with lift-to-drag ratio. Heat load is more significantly affected by entry flight path angle.

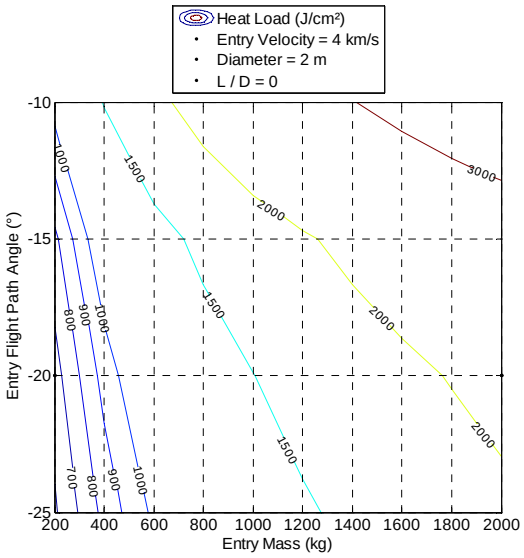


**Figure 17 Heat load as a function of entry mass and flight path angle.**

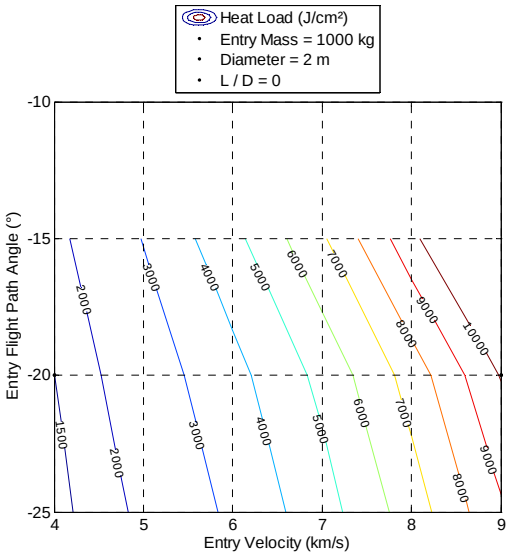


**Figure 18 Heat load as a function of entry velocity and flight path angle.**

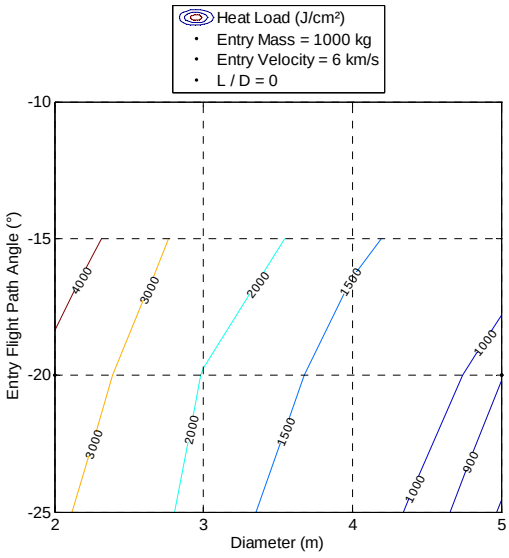


**Figure 19 Heat load as a function of aeroshell diameter and entry flight path angle.**

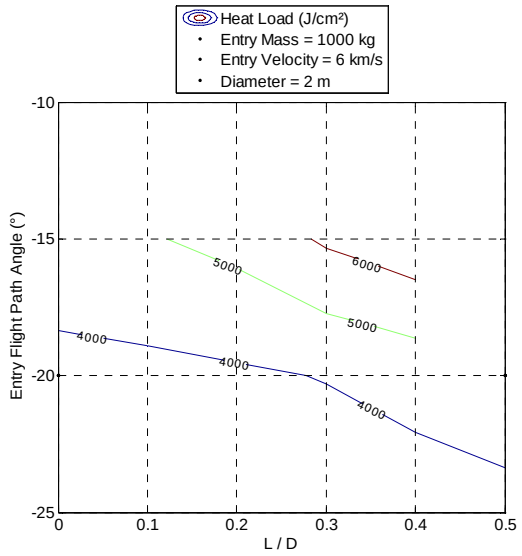


**Figure 20 Heat load as a function of lift-to-drag ratio and entry flight path angle.**

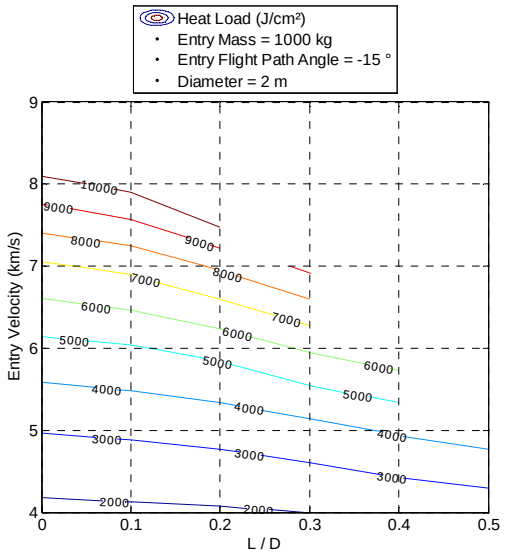


**Figure 21 Heat load as a function of lift-to-drag ratio and entry velocity.**

### D. Mach 2 Altitude

Figure 22 shows that the altitude at which Mach 2 is reached is strongly affected by the entry flight path angle and less significantly affected by entry flight path angle when entry velocity, aeroshell diameter, and the lift-to-drag ratio of the planetary probe are all fixed. Figure 23 shows that for a ballistic entry the Mach 2 altitude is not strongly affected by entry velocity, but the altitude at which Mach 2 is reached is impacted by the entry flight path angle. As entry flight path angle steepens, the altitude at which Mach 2 is reached decreases when the entry mass, aeroshell diameter, and the lift-to-drag ratio of the planetary probe are all fixed.

As stated above, a steeper entry flight path angle decreases the Mach 2 altitude. This is shown again in Figure 24. Figure 24 also shows that the Mach 2 altitude increases as the aeroshell diameter of the probe increases. The larger diameter allows the planetary probe to slow down higher in the atmosphere and thus remain at a higher altitude when Mach 2 is reached.

For a fixed entry flight path angle, Figure 25 shows that a higher lift-to-drag ratio allows higher altitudes to be reached at Mach 2 when entry mass, entry velocity, and aeroshell diameter are all fixed. In the region to the right of the line connecting the point (-15°,0.1) to the point (-25°,0.2), skipping begins to occur. Skipping trajectories give rise to the higher altitude islands seen on the contour plot such as the island around the point (-20°,0.2).

The effect of skipping is again evident in Figure 26. Alternatively, bank angle control could be used with a planetary probe flying a lifting trajectory to prevent skipping.

Combinations of higher entry velocity, shallower entry flight path angles and higher lift-to-drag ratios generally lead to skipping.

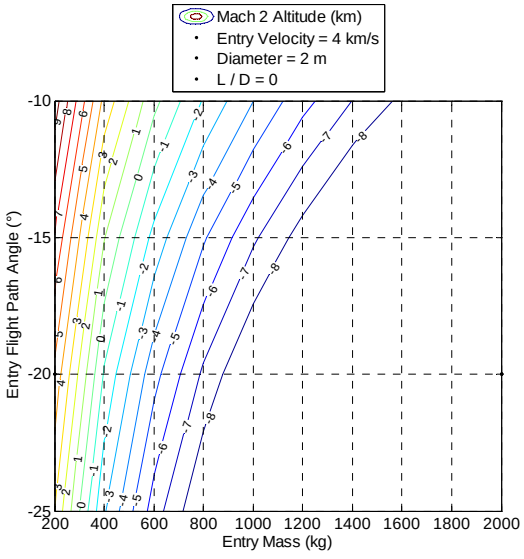


**Figure 22 Mach 2 altitude as a function of entry mass and flight path angle.**

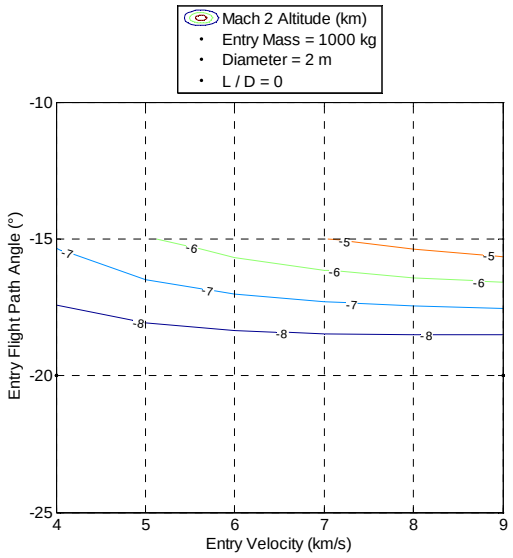


**Figure 23 Mach 2 altitude as a function of entry velocity and flight path angle.**

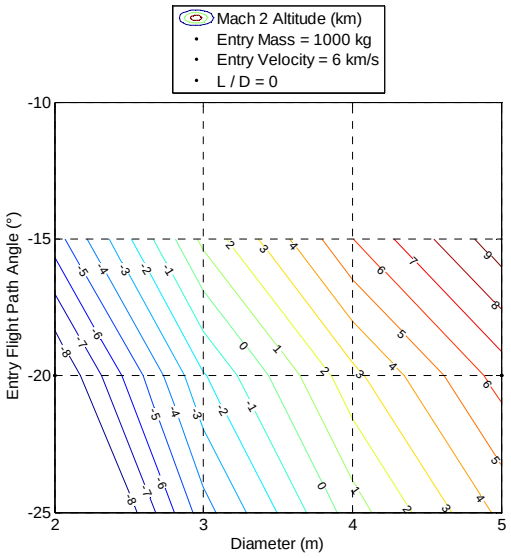


**Figure 24 Mach 2 altitude as a function of aeroshell diameter and entry flight path angle.**

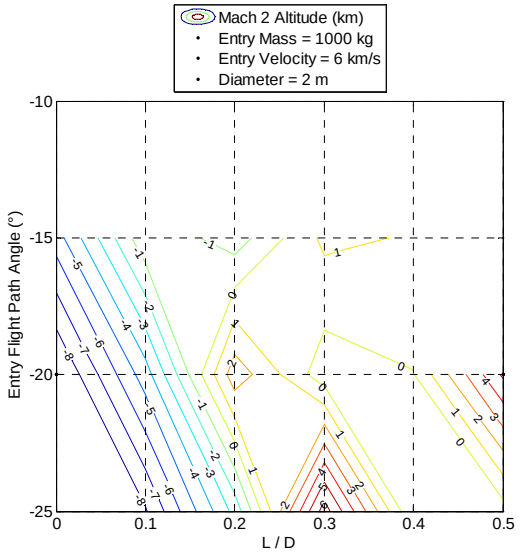


**Figure 25 Mach 2 altitude as a function of lift-to-drag ratio and entry flight path angle.**

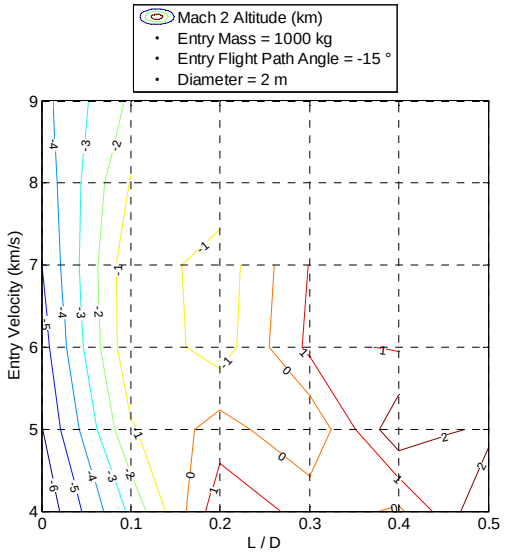


**Figure 26 Mach 2 altitude as a function of lift-to-drag ratio and entry velocity.**

## IV. Conclusions

Contour plots (or pork-chop plots as they are called by interplanetary mission designers) can be used to study trends in entry trajectories when major variables change. However, the number of independent major variables is more than can easily be represented in 2- or 3-dimensional plots, which makes looking at the effects of multiple variables difficult. Collections of contour plots such as that in the appendix can form the basis of entry mission design handbooks (the equivalent of interplanetary mission design handbooks).

## References


[1]Braun, R.D., Manning, R.M., "Mars Exploration Entry, Descent and Landing Challenges," *2006 IEEE Aerospace Conference*, IEEEAC paper #0076, Big Sky, Montana, March 2006.

[2]Ingoldby, R. N., Michel, F. C., Flaherty, T. M., Doty, M. G., Preston, B., Villyard, K. W., Steele, R. D., "Entry Data Analysis for Viking Landers 1 and 2 Final Report", Martin Marietta Corp., NASA TN 3770218, NASA CR 159388, November 1976.

[3]Spencer, D.A., Blanchard, R.C., Braun, R.D., Kallemeyn, P.H., Thurman, S.W., "Mars Pathfinder Entry, Descent, and Landing Reconstruction", *Journal of Spacecraft and Rockets*, Vol. 36, No. 3, May-June 1999.

[4]Desai, P.N., Knocke, P.C., "Mars Exploration Rovers Entry, Descent, and Landing Trajectory Analysis," *AIAA/AAS Astrodynamics Specialist Conference and Exhibit*, AIAA 2004-5092, Providence, Rhode Island, August 16-19, 2004.

[5]POST, Program to Optimize Simulated Trajectories, Ver. 5.2, NASA Langley Research Center, Hampton, Virginia, Martin Marietta Corporation, Denver, Colorado, 1997.

[6]Gnoffo, P., Braun, R.D., Weilmuenster, K.J., Mitcheltree, R.A., Engelund, W.C., Powell, R.W., "Prediction and Validation of Mars Pathfinder Hypersonic Aerodynamic Database," *7th AIAA/ASME Joint Thermophysics and Heat Transfer Conference*, AIAA 98-2445, Albuquerque, New Mexico, June 1998.

[7]Mars-GRAM, Mars Global Reference Atmospheric Model, Ver 2005, Computer Sciences Corporation, Huntsville Alabama, NASA Marshall Spaceflight Center, Alabama, 2005,

[8]Tauber, M.E., Sutton, K., "Stagnation-Point Radiative Heating Relations for Earth and Mars Entries", *Journal of Spacecraft and Rockets*, Vol. 28, pp. 40-42, January-February 1991.

[9]"Mars, The Red Planet Reference Map," Copyright © 2001 *National Geographic Society*, Washington, DC.